Journal of Alloys and Compounds 735 (2018) 2471–2478

Contents lists available at ScienceDirect

Journal of Alloys and Compounds

journal homepage: http://www.elsevier.com/locate/jalcom

Structural and electronic properties of Al-doped ZnO semiconductor nanopowders: Interplay between XRD and PALS experiments and first-principles/DFT modeling

L.C. Damonte, G.N. Darriba*, M. Rentería

Departamento de Física and Instituto de Física La Plata (IFLP, CONICET La Plata), Facultad de Ciencias Exactas, Universidad Nacional de La Plata, CC 67, 1900 La Plata, Argentina

ARTICLE INFO

Article history:
Received 26 June 2017
Received in revised form
25 October 2017
Accepted 6 November 2017

Keywords:
Positron spectroscopies
X-ray diffraction
Computer simulations
Solid state reactions
Electronic properties
Semiconductors

ABSTRACT

A combined experimental and novel theoretical *ab initio* structural and electronic study was performed in order to characterize ZnO semiconductor nanopowders doped with Al atoms. For this, powder mixtures of ZnO and metallic Al in adequate proportions yielding different contents of Al (5, 10, and 30 at. %) were prepared by mechanical milling. The systems were characterized by X-ray diffraction and positron annihilation lifetime spectroscopy measurements. Additionally, combining two first-principles methods based on the Density Functional Theory (DFT) we calculated the final equilibrium structures for different concentrations of Al dopants and Zn vacancies in ZnO, predicting afterwards the characteristic positron annihilation lifetimes at these equilibrium structures. In addition to the structural relaxations, the *ab initio* predictions of the electronic properties in the studied systems help us to understand deeper the origin and characteristics of different positrons traps.

This experimental and *ab initio*/DFT combined study allows to verify the dopant incorporation into the ZnO *wurtzite* structure and to extract the maximum information from the experimental data, giving an insight into the different defect complexes and their influence in the structural and electrical properties.

1. Introduction

Zinc oxide is a II-VI semiconductor suitable for numerous technological applications such as optoelectronic devices, solar cells, gas sensors [1,2], etc. It is well known that the addition of different dopants, both as acceptors or donors, improves its performance. Many preparation methods were applied to obtain pure and doped ZnO nanostructures, such as sol-gel [3], chemical synthesis [4], electrodeposition [5], and mechanical milling [6]. In addition, its peculiar properties can be customized by the morphology and, naturally, by the presence of defects induced by each fabrication method.

Mechanical milling has proved its capability to obtain composites, amorphous alloys, intermetallics synthesis and a variety of nanomaterials at room temperature [7]. It was also successfully applied to obtain ZnO nanopowders [8] and trivalent dopants incorporation in them [9]. However, during milling different kinds of defects can be simultaneously induced, which many times may be non-desirable [10].

Positron annihilation lifetime spectroscopy (PALS) is an extremely sensitive technique to open volume defects and to their evolution with mechanical and thermal treatments [11]. PALS has been widely applied to sense defects in ZnO and other semiconductors. Although its high ability to probe the origin and the characteristics of defects, the concurrently presence of different kind of them makes extremely difficult their precise analysis. In consequence, it will be essential to complement the experimental data developing a novel strategy based in very accurate and precise theoretical *ab initio* calculation of positron lifetimes in solids in the framework of the Density Functional Theory (DFT).

In previous works [9,12] structural and optical properties on mechanically doped ZnO from different starting materials were investigated. It was demonstrated there that positron annihilation lifetime spectroscopy constitutes an effective tool to sense dopant incorporation into ZnO semiconductor powders through the average lifetime evolution with milling time.

In the present work, a step forward was performed trying a combined experimental and *ab initio* structural and electronic

* Corresponding author.
E-mail address: darriba@fisica.unlp.edu.ar (G.N. Darriba).

https://doi.org/10.1016/j.jallcom.2017.11.072
0925-8388/

study in order to characterize the Al-doped ZnO semiconductor. Al-doped ZnO nanopowders obtained by mechanical milling were characterized by X-ray diffraction (XRD) and PALS measurements. The *ab initio* study was performed combining two different methods based on the Density Functional Theory (DFT). In this double approach the equilibrium structures of the doped systems (i.e., final atomic positions) were obtained applying the Full-Potential Augmented Plane Wave plus local orbitals (APW+lo) method, embodied in the WIEN2k code. After this, the characteristic semiconductor lifetimes were predicted, at these equilibrium structures, using the Multigrid Instead of the K-spAce (MIKA) program. In addition, the structural relaxations and the electronic density of states (DOS) were evaluated with the aim to elucidate the structural and electronic distortions introduced by the different defects (Al substitutional, Zn vacancies) in the ZnO structure and their influence on the positron lifetimes.

Both theoretical and experimental results were compared in order to allow the extraction of maximum information from the experimental data, as well as to get insight into the structural and electronic properties of the doped semiconductor and their influence on devices performance.

2. Experimental

2.1. Sample preparation and XRD and PALS measurements

Mixtures of ZnO (99.99% purity) and Al (99.5% purity, 325 mesh) commercial powders (Alfa Aesar Johnson Matthey Co.) were prepared at stoichiometric quantities such as to obtain a 5, 10 and 30% at. of aluminum in ZnO, labeled hereafter as ZOA_5, ZOA_10, and ZOA_30, respectively. The samples were then milled at a Retsch MM2 horizontal vibratory mill inside a steel cylinder (8 cm^3) with one steel ball (radius of 5 mm, being the ball to powder weight ratio of 10:1) at milling times of 1, 4, and 16 h.

Characterization of the crystal structures of the resulting samples was done by XRD performed in an X-Pert Philips PW 3011/20 diffractometer with *Cu* K_α radiation in the $20^\circ < 2\theta < 80^\circ$ range, with steps of 0.05° every 2 s. Each X-ray diffraction pattern was analyzed by the Rietveld refinement method using the FULLPROF [13] program with the pseudo-Voigt Thompson-Cox-Hasting peak shape [14].

The powders with a certain dopant concentration were compacted into two disk-shaped pellets (diameter 8 mm) in order to be carried on the PALS set-up.

Positron Annihilation Lifetime Spectroscopy is based on the measurement of the positron lifetime inside the material under study. Since in matter a positron and an electron mainly annihilate by the emission of two gamma rays of 511 keV, the positron has the capability to sense electron density in the bulk of the material. The measured positron lifetime is related to the open volume defect size allowing characterizing the defect structure of the material under study. Ordinarily, short lifetimes (of the order of 250 ps) describe the crystalline material. Lifetimes in the range of about 300–600 ps show the existence of regions having point defects or small association of point defects. Long lifetimes (higher than 1000 ps) reveal the occurrence of large depleted volumes (cavities) inside the material.

The radioactive source (sodium solution $^{22}NaCl$, with an activity of 10 μCi) deposited onto a kapton foil (1.42 g/cm^3) was sandwiched between each pair of sample pellets. PALS spectra were collected at room temperature (RT) with a conventional fast-fast coincidence system with two (BaF_2) scintillating detectors (FWHM, 285ps), acquiring 3×10^6 counts per spectrum [9]. The source contribution (a signal of 386 ps with 15% intensity is assigned to the kapton foil and a second one of around 1 ns with less than 1% intensity is due to annihilation in the surroundings of the source) and the response function were evaluated from a reference sample (Hf metal) using the RESOLUTION code [15]. PATFIT code [15] was used to analyze the PALS results.

2.2. Experimental results

2.2.1. XRD

Fig. 1 shows the XRD patterns for all samples as a function of milling time. After 1 h of mechanical milling, the reflections of the hexagonal ($P6_3mc$) crystal structure of zinc oxide (described in detail in Section 3.1) are mainly seen. The presence of metallic Al

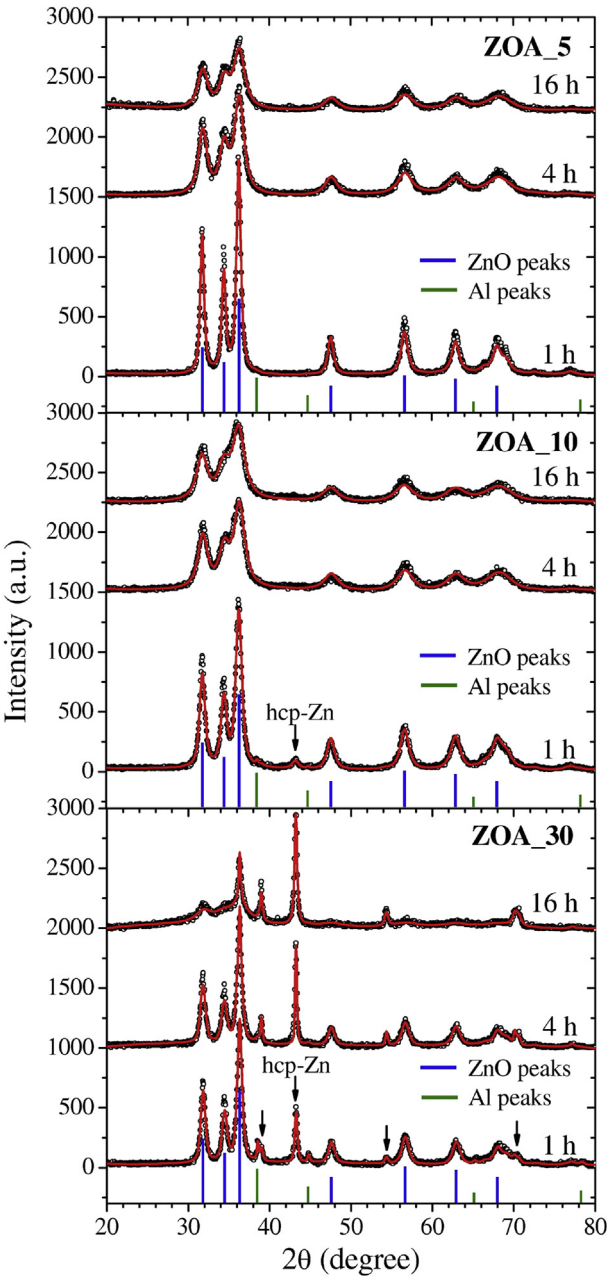

Fig. 1. XRD diffraction patterns at different milling time for ZOA_5 (up), ZOA_10 (middle), and ZOA_30 (down) samples. ZnO (blue lines) and Al (green lines) diffraction peaks are indicated. The arrows indicate the presence of hcp-Zn peaks. (For interpretation of the references to color in this figure legend, the reader is referred to the web version of this article.)

($2\theta \approx 38°$, main line of c-Al) is observed in all samples (presenting higher intensity for larger doping concentrations) while metallic Zn ($2\theta \approx 43°$, corresponding to hcp-Zn) is only present in ZOA_10 and, with higher intensity, in ZOA_30. For longer milling times, these two metallic elements are not detected by X-ray diffraction for the 5 and 10 at% Al-doped samples, which may be an evidence of Al incorporation into the ZnO host lattice.

The XRD pattern for ZOA_30 after 16 h of milling looks substantially different. The main diffraction lines correspond to the hcp-Zn crystal phase coming from reduction of Zn from *wurtzite* ZnO.

Unit cell constants and grain size for all the samples, obtained by the Rietveld fitting procedure for the *wurtzite* phase, are displayed in Table 1. No major changes are observed in the lattice parameters with milling time for all compositions. On the other hand, broadening of the diffraction peaks as milling time increases is observed, implying the diminution of the ZnO crystallite for all the dopant concentrations. In effect, this behavior is correlated with the monotonous decrease of the coherent scattering domain size L (see Table 1) as a function of increasing milling time. It is worthwhile to note that a similar feature (for both, lattice parameters and L) was observed in undoped ZnO when is subjected to mechanical work, as it was stated previously [8].

2.2.2. PALS

Different phases developing in the samples and their evolution with milling time and Al concentration were characterized by positron annihilation lifetime measurements. The lifetime spectra for all samples were decomposed into three exponential decays according to:

$$n(t) = \sum_i I_i \exp(-t/\tau_i),$$

being the relative intensities I_i normalized to unity, $\sum_i I_i = 1$, and τ_i the positron lifetime. After background subtraction and convolution with the experimental time-resolution function (the response function), the parameters that characterized each positron state, i.e. the annihilation rate $\lambda_i = 1/\tau_i$ and its relative intensity I_i, are obtained by means of the POSITRONFIT fitting program [15].

Normally, II-VI semiconductor compounds exhibit two-lifetime-components spectra since intrinsic and extrinsic defects (such as vacancies, interstitials, etc.) usually introduced during crystal growth and doping are unavoidable [11]. The shorter component (τ_1) comes, usually, from free annihilation of positrons in the delocalized bulk state and the other (τ_2) from trapped positrons at defects. In our case, the longest component τ_3 is ascribed to ortho-positronium annihilation formed in large voids present in the material. In the present study, this component (~1100 ps) maintains its low intensity I_3 in all the analyzed samples, so it will not considered in the forthcoming discussion.

Fig. 2 shows the resulting lifetime parameters for all samples as milling time increases. At first sight, ZOA_5 and ZOA_10 display a similar behavior but different from the ZOA_30 one.

Table 1
Lattice parameters (a, c) and coherent scattering domain size (L) obtained from Rietveld refinements for all Al-doped ZnO samples, as a function of the milling time.

Time (h)	ZOA_5			ZOA_10			ZOA_30		
	a (Å)	c (Å)	L (nm)	a (Å)	c (Å)	L (nm)	a (Å)	c (Å)	L (nm)
1	3.250	5.206	18.3	3.25	5.207	17.8	3.250	5.208	17.8
4	3.249	5.205	15.0	3.25	5.206	15.3	3.248	5.207	16.0
16	3.250	5.204	14.8	3.25	5.204	14.0	3.249	5.204	13.4

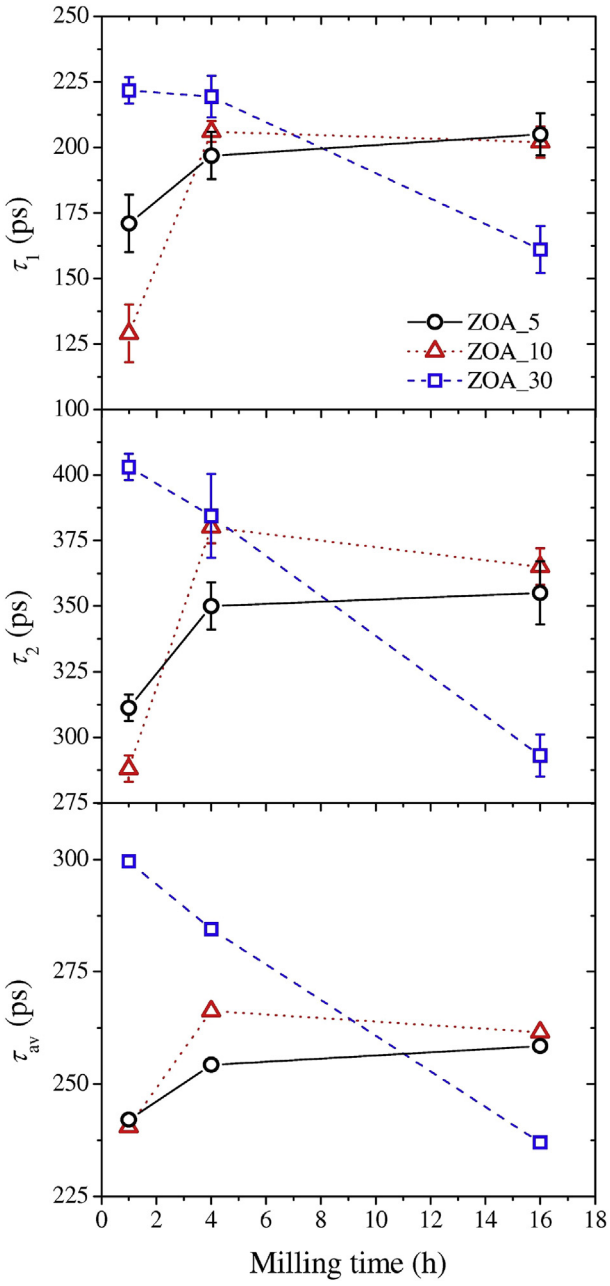

Fig. 2. Positron annihilation lifetimes τ_1 (up), τ_2 (middle), and τ_{av} (down) at different milling time for ZOA_5, ZOA_10, and ZOA_30 samples.

After 1 h of milling, the shortest lifetime τ_1 clearly differs for each dopant concentration, and even has a different value from that corresponding to pure ZnO bulk. In disordered systems, smaller vacancies (like Zn monovacancies, V_{Zn}) or shallow positron traps (like oxygen vacancies, V_O) in ZnO may be mixed with τ_1 [10,12]. Since the known values for bulk lifetimes for ZnO and metallic Al are 158 ps and 162 ps, respectively [16,17], this first component should be considered a weighted average of all the above mentioned possible contributions (i.e, ZnO, Al, V_{Zn}, and V_O) in the case of ZOA_5 (yielding a value of around 170(12) ps, see Fig. 2). For ZOA_10 and ZOA_30 some slight contribution from hcp-Zn should be present, in addition to the previous weighted average, since metallic Zn was observed after 1 h milling by XRD. So, the shortest lifetime component (τ_1, at around 129 ps for ZOA_10 and 222 ps for ZOA_30) generally attributed to free annihilation of positrons in the

bulk of the pure (undoped) host material, must be considered here as a weighted average of free positrons in undoped ZnO and trapped positrons in different crystal phases and point defects (hcp-Zn, V_{Zn}, Vo, etc.) [18].

At the same stage of milling (1 h), the second lifetime τ_2 varied from 288 for ZOA_10 to 408 ps for ZOA_30, indicating different positron traps for each sample. Similar lifetime range of values for the second component were observed in ZnO mixtures with Mg, Cd and Al [9], which may originate from clustered V_{Zn} or from some complexes of V_{Zn} with large open volume.

However, after 4 h of milling all the samples display almost the same positron parameters, i.e, lifetimes and their respective intensities.

For longer milling times (16 hs), there are substantial differences between ZOA_30 and the other two compositions for τ_1 and τ_2. While the annihilation parameters corresponding to ZOA_5 and ZOA_10 remains similar to those obtained in the previous milling step (4 hs), both lifetimes τ_1 and τ_2 drastically diminish for the 30 at. % (ZOA_30) doped sample.

It comes from the above discussion that different positron traps with similar lifetime values contribute to both components, so the average positron lifetime $\tau_{av} = \sum_i \tau_i I_i$ constitutes a more accurate parameter to evaluate defects. The obtained values for τ_{av} are also shown in Fig. 2 (bottom). The observed behavior clearly illustrates that mechanically-induced defects for the ZOA_30 doped sample are different than those for the less doped ones.

During initial stages of milling many defects are introduced with the generation of high strain [8]. It is generally accepted that lifetimes of 220 ps and 245 ps are ascribed to vacancies at dislocations and monovacancies in plastic deformed Al [17]. In addition, values of positron lifetimes originating from V_O and Zn monovacancy (V_{Zn}) in ZnO of 180 ps and 230 ps, respectively, were experimentally found [19,20]. In the case of mixtures of different structures, such as in our case, a high crystalline disorder is also generated given place to defects association. Prolonged milling times give rise to different mechano-chemical reactions yielding a homogeneous material [7].

In view of the above discussion and with the aim to clarify the origin and characteristics of the induced defects in the studied doped samples, theoretical calculations of positron annihilation lifetimes in different crystal structures and point defects were necessary, whose results are described in the next section.

3. Ab initio calculations

3.1. Crystal structure and calculation details

We present here and discuss the electronic structure DFT-based *ab initio* calculations in Al-doped ZnO and in ZnO with Zn vacancies. In order to simulate the different concentrations of Al impurities and Zn vacancies we used different supercells (SC) containing 2 ($2 \times 1 \times 1$ SC), 4 ($2 \times 2 \times 1$ SC), 8 ($2 \times 2 \times 2$ SC), and 16 ($4 \times 2 \times 2$ SC) unit cells of ZnO (see Fig. 3). The ZnO unit cell has a *wurzite* hexagonal geometry (space group $P6_3mc$) with $a = b = 3.2501$ Å and $c = 5.2071(1)$ Å, containing two Zn atoms at positions (0;0;0) and (1/3;2/3;1/2), and two O atoms at positions (0;0; u) and (1/3;2/3; u+1/2), with $u = 0.3817(3)$ [21]. The Zn atoms are coordinated with four nearest neighbors (ONN) oxygen atoms, three at 1.975 Å (O1, O2 and O3) and one at 1.988 Å (O4), located at the vertices of a tetrahedron slightly elongated along the c crystal axis.

To simulate the Al-doped ZnO systems we replaced in the $2 \times 1 \times 1$, $2 \times 2 \times 1$, $2 \times 2 \times 2$, and $4 \times 2 \times 2$ SCs one Zn atom by an Al one, obtaining 1/4, 1/8, 1/16 and 1/32 cationic dilution, using the notation ZOA(1/4a), ZOA(1/8a), ZOA(1/16), and ZOA(1/32) for these systems, respectively. Using the $2 \times 2 \times 2$ SC and replacing 3 Zn atoms by 3 Al atoms we obtain 3/16 cationic dilution of the Al impurity, called ZOA(3/16). Additionally, for 1/4 and 1/8 dilution, we have different configurations of Al impurities employing the $2 \times 2 \times 2$ SC, and called this as ZOA(1/4b) ZOA(1/8b). All the configurations described above are the initial (unrelaxed) structures (i.e., the initial atomic positions) used as "starting point" to find the final equilibrium structures for each Al-doped ZnO system. Schematic representations of the unrelaxed Al-doped ZnO systems are shown in Fig. 4.

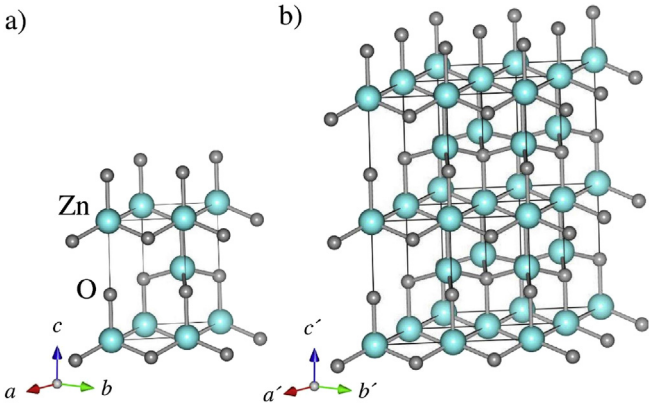

Fig. 3. a) Unit cell of *wurtzite* ZnO, b) $2 \times 2 \times 2$ SC with $a' = 2a$, $b' = 2b$ and $c' = 2c$.

To simulate the Zn vacancies in ZnO we removed one Zn atom in the $2 \times 1 \times 1$ SC, $2 \times 2 \times 1$ SC, and $2 \times 2 \times 2$ SC obtaining 1/4, 1/8, and 1/16 cationic dilution, respectively. And we call these systems as V_{Zn}(1/4), V_{Zn}(1/8) and V_{Zn}(1/16), respectively. As in the Al-doped systems, all the configurations described here are the initial (unrelaxed) structures used as "starting point" to find the final equilibrium structures for each system with Zn vacancies.

In order to obtain the final equilibrium atomic positions and the corresponding electronic structure in Al-doped ZnO and in ZnO with Zn vacancies systems we performed a complete optimization of the atomic positions of all atoms in the corresponding SC, finding the equilibrium structures (relaxed systems). For this, we employed the FP-APW+lo method [22] embodied in the WIEN2k code [23]. In this method, the wave functions are expanded in spherical harmonics into non-overlapping spheres centered at the atoms, and in plane waves in the interstitial region. The cut-off parameter of the plane waves in the interstitial region was $R_{MT}K_{max} = 7$, where R_{MT} is the smallest radius of the non-overlapping spheres and K_{max} is, in the reciprocal space, the maximum modulus of the lattice vectors. The R_{MT}(Al), R_{MT}(Zn), and R_{MT}(O) were 0.93 Å, 0.99 Å, and 0.87 Å, respectively, and we took 70 k-points in the first Brillouin zone of the reciprocal space. Exchange and correlation effects were treated using the local-density approximation (LDA) [24], and the generalized gradient approximation (PBE-GGA) [25]. In order to obtain the equilibrium structures of the SCs, all atoms were displaced from their initial positions following a Newton dampened scheme [26], repeating it until the forces on the atoms were below a tolerance value of 0.01 eV/Å.

The positron annihilation lifetime τ was calculated, at the equilibrium structures predicted by WIEN2k, using the MIKA/Doppler program [27], based in the so-called atomic superposition (ATSUP) method [28]. In this method, the electron density is simply computed as the sum of atomic electron densities in a non-self-consistent way. Exchange and correlation effects were treated using the local density approximation (LDA) and the generalized gradient approximation (GGA), and the enhancement factors of the electron density at the positron was treated as proposed by Boronski and Nieminen (BN) [29], by Arponen and Pajanne (AP1) [30],

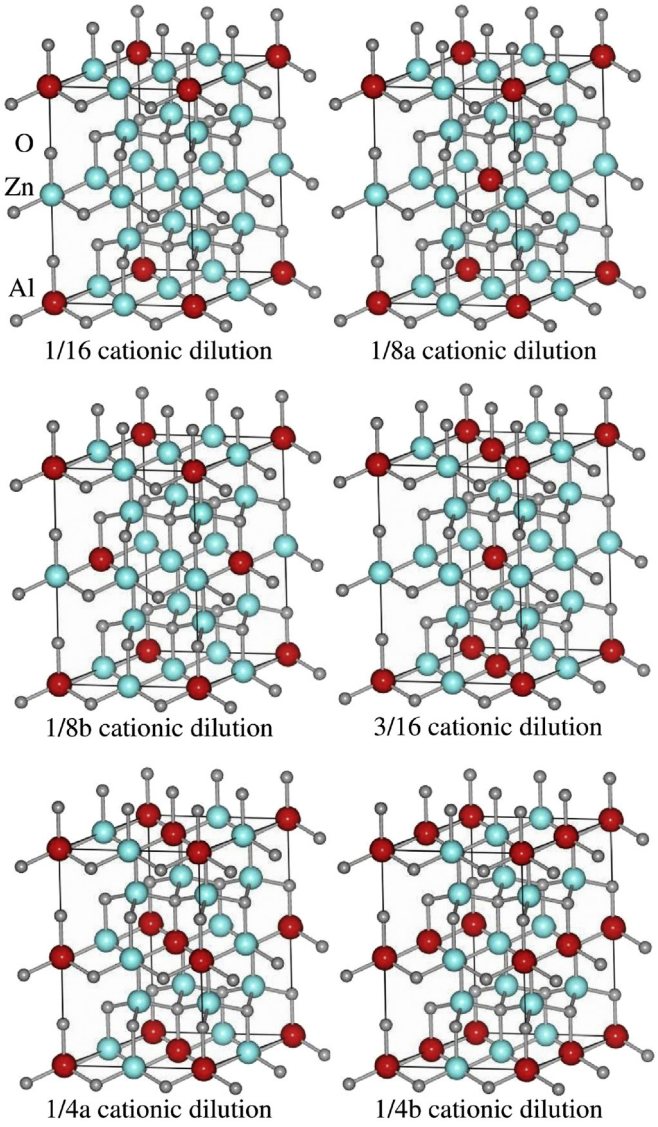

Fig. 4. Schematic dilutions used as "starting point" in all the *ab initio* calculations in Al-doped ZnO. For 1/4 and 1/8 cationic dilutions there are two initial locations of the Al impurity (red spheres), labeled as 1/4a and 1/4b, and 1/8a and 1/8b, respectively. (For interpretation of the references to color in this figure legend, the reader is referred to the web version of this article.)

and by Barbiellini et al. (AP2) [31].

The electronic structure and the positron annihilation lifetimes were also predicted for the undoped (pure) ZnO system, in order to be able to evaluate the changes introduced by both kinds of defects (Al or Zn vacancies).

3.2. Results and discussion

The substitution of a lattice native Zn atom by an Al impurity induces considerable forces acting on Al and its neighboring atoms, as well as, in a lesser extent, on the rest of the atoms of the SC. To consider this effect in the calculations we found the final atomic equilibrium positions, obtained after the already mentioned full relaxation process, taking into account the displacement of all the atoms of the SC. In all the studied Al-doped ZnO systems, when a Zn atom is replaced by an Al one, the bond-length of the four nearest oxygen atoms neighbors to the Al atom result shorter than those of the native Zn. In Table 2 we compare the Al-ONN bond-lengths at the final equilibrium positions for all doped systems studied with the Zn-ONN bond-lengths for undoped ZnO, in order to evaluate the structural distortions introduced by the Al atoms in the ZnO host lattice.

As we can see in Table 2 comparing the Zn-ONN and Al-ONN bond-lengths, the substitution of a Zn atom by an Al one produces, in all Al-doped ZnO systems, anisotropic contractions in the ONN bond-lengths. For ZOA(1/32), ZOA(1/16) and ZOA(1/8b) the tetrahedron formed by the ONN is preserved but shortened along the c crystal axis, becoming a regular tetrahedron. In the rest of the Al-doped systems, this tetrahedron shape is distorted. The structural distortions, i.e. the contractions in the Al-ONN bond-lengths, could be expected from the analysis of the ionic radii sizes, since the ionic radius of Al^{3+} is 0.39 Å, which is smaller than the 0.60 Å value for Zn^{2+}, both quoted values corresponding to four-fold coordination. This structural behavior related with the ionic radii relative sizes of an impurity and the native host cations was already observed in some Ta- and Cd-doped semiconductor oxides, and was deeply discussed in Ref. [32]. Besides the local structural relaxations introduced by the impurity, there are not appreciable changes in the lattice parameters as a function of the impurity dilution within the precision of the calculations, in agreement with the XRD measurements reported in Table 1.

On the other hand, when a Zn atom is removed from the ZnO structure, in order to simulate diluted Zn vacancies, the distances from the Zn vacant site to its ONN atoms increase anisotropically with respect to the distances that have this removed Zn atom with its ONN in undoped ZnO (see Table 3). In all cases, the tetrahedron formed by these ONN in the doped relaxed system is strongly distorted.

In addition to the structural relaxation, the substitution of a Zn atom by an Al impurity and the generation of Zn vacancies induce strong changes in the electronic structure of the ZnO semiconductor. In Fig. 5 we compare the electronic density of states (DOS) of undoped ZnO with those corresponding to Al-doped and with Zn vacancies in ZnO, for ZOA(1/16) and V_{Zn}(1/16) systems, respectively.

As we see, comparing Fig. 5a and 5b, the substitution of a Zn atom by an Al one introduces a delocalized "donor" state located at the bottom of the conduction band, giving to the Al-doped system a metallic character. Integration of the total DOS of the occupied states in the conduction band gives a value of 1.01 e^-, in agreement with the nominal single donor character of Al^{3+} substituting a Zn^{2+} atom in ZnO. In addition to this change in the electronic structure, the Al atom introduces impurity levels located at the bottom of the valence band (as we see in Fig. 5b). On the other hand, comparing Fig. 5a and 5c we can see that the removal of a Zn atom from the ZnO SC introduces a localized "acceptor" level located at the top of the valence band. In this case, integration of the total DOS of the unoccupied states in the valence band gives a value of 1.98 e^-, in agreement with the double acceptor character of the removed Zn^{2+} atom in ZnO.

As a first step in the prediction of the positron annihilation lifetime τ, and before to study the Al-doped ZnO and ZnO with Zn vacancies systems, we performed calculations for pure (undoped) ZnO (at the experimental lattice and internal parameters) using the LDA and the GGA approximations, and the BN, AP1, and AP2 enhancement factors of the electron density at the positron, using the MIKA/Doppler program. In Table 4 we show the predicted τ values for undoped ZnO using a high frequency dielectric constant $\varepsilon_\infty = 4$. Comparing the predicted results with the experimental bulk value obtained in a single crystalline sample of ZnO [18] (see Table 4) we can see that the predicted τ is in perfect agreement with the experimental value when using the LDA approximation

Table 2
Zn-ONN bond-lengths (d Zn-Oi) for undoped ZnO and *ab initio* predicted Al-ONN distances (d Al-Oi) in Al-doped ZnO systems at the atomic equilibrium positions. For undoped ZnO we use the experimental lattice and internal parameters of Ref. [21].

Undoped ZnO				
	d Zn-O1 (Å)	d Zn-O2 (Å)	d Zn-O3 (Å)	d Zn-O4 (Å)
	1.975	1.975	1.975	1.988
Al-doped ZnO				
	d Al-O1 (Å)	d Al-O2 (Å)	d Al-O3 (Å)	d Al-O4 (Å)
ZOA(1/32)	1.808	1.808	1.808	1.804
ZOA(1/16)	1.814	1.814	1.814	1.802
ZOA(1/8a)	1.808	1.808	1.805	1.807
ZOA(1/8b)	1.806	1.806	1.806	1.797
ZOA(3/16)	1.850	1.850	1.791	1.790
ZOA(1/4a)	1.846	1.846	1.783	1.795
ZOA(1/4b)	1.848	1.848	1.786	1.793

Table 3
Zn-ONN bond-lengths (d Zn-Oi) for undoped ZnO and *ab initio* predicted distances from the Zn vacant site (V_{Zn}) to its ONN (d V_{Zn}-Oi) in ZnO with Zn vacancies systems at the atomic equilibrium positions. For undoped ZnO we use the experimental lattice parameters of Ref. [21].

Undoped ZnO				
	d Zn-O1 (Å)	d Zn-O2 (Å)	d Zn-O3 (Å)	d Zn-O4 (Å)
	1.975	1.975	1.975	1.988
Zn vacancies in ZnO				
	d V_{Zn}-O1 (Å)	d V_{Zn}-O2 (Å)	d V_{Zn}-O3 (Å)	d V_{Zn}-O4 (Å)
V_{Zn} (1/16)	2.132	2.119	2.119	2.035
V_{Zn}(1/8)	2.132	2.154	2.154	2.060
V_{Zn}(1/4)	2.127	2.069	2.069	2.091

and the BN enhancement factor. Additionally, using this set up parameters, we predicted a value of $\tau = 149$ ps for hcp-Zn, in agreement with the experimental ones reported in Ref. [33].

For this reason, we used LDA, BN, and $\varepsilon_\infty = 4$ for all calculations reported in what follows for Al-doped ZnO and ZnO with Zn vacancies.

In Table 5 we present the predicted τ for all the studied Al-doped ZnO systems, whereas in Table 6 we show the results for all the Zn vacancy concentrations in ZnO. In both tables, the predicted τ values were calculated at the atomic positions corresponding to undoped ZnO (unrelaxed structures) and once the atomic equilibrium positions were achieved in a self-consistent way (relaxed structures).

As we can see in Table 5, when a Zn atom is replaced by an Al one (unrelaxed structure), τ is basically the same, almost independently of the Al concentration. Once the Al is incorporated into the ZnO structure at substitutional Zn sites and all the atoms achieve their equilibrium positions, a slight increasing tendency of τ with the Al concentration is observed. This little change in τ could be attributed to the distortion of the tetrahedron formed by the ONN at high Al concentration (see Table 2). Nevertheless, and for simplicity, these systems, i. e., Al incorporated into the ZnO structure, will be referred as ZOA, independently of the Al concentration, and assuming an average positron annihilation lifetime of 160 ps.

Oppositely to the Al-doped ZnO case, when a Zn atom is removed from the unrelaxed ZnO structure, τ changes and its value depend on the vacancy concentration (see Table 6), i.e., the electronic changes (since the structural relaxation effect is frozen) play a key role in the τ value. As we see in Table 6, when a Zn vacancy is involved, the positron lifetime also strongly depends on the structural relaxation of the ZnO host, due to the fact that these relaxations result stronger and more anisotropic than those produced in the Al-doped ZnO systems (see Tables 2 and 3).

In addition, the positron lifetime values displayed in Table 6 for relaxed structures are in agreement with the experimental

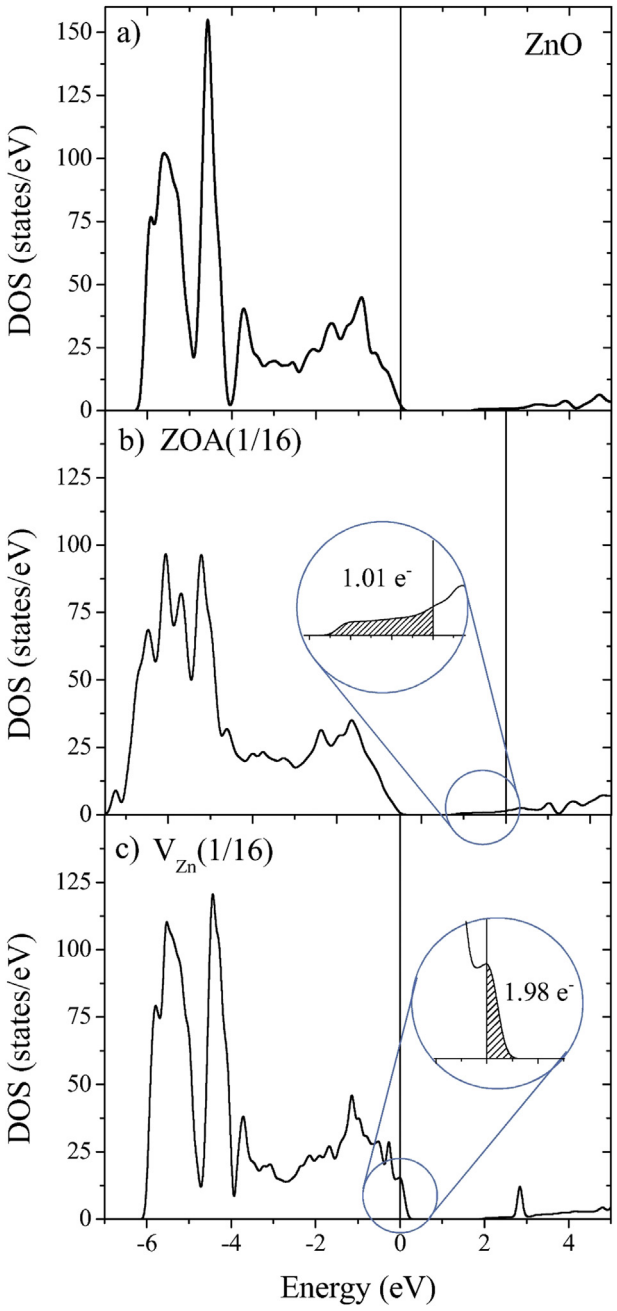

Fig. 5. Total electronic density of states (DOS) for: a) undoped ZnO, b) Al-doped ZnO (ZOA(1/16)), and c) Zn vacancy in ZnO (V_{Zn}(1/16)). The vertical line indicates the last occupied state. In b) and c) donor and acceptor states are zoomed, respectively.

determinations reported by other authors for a positron trapped at Zn monovacancies [18,20].

4. Discussion of evolving species in the samples

In Fig. 6 we compare the experimental results for τ_1 with an average of lifetime *ab initio* values predicted for different systems (all with the same weight). As shown in this figure, the experimental results for ZOA_5 and ZOA_10 could be associated, after 4 and 16 h of milling, with the averages of the *ab initio* τ values predicted for Al incorporated at substitutional Zn sites (ZOA) and at Zn vacancies in the ZnO structure. Particularly, when the cationic concentration of Zn vacancies is 1/4 (grey stars) the agreement is

Table 4
Positron annihilation lifetime τ in ps predicted for undoped ZnO bulk using the LDA and the GGA approximations, and the BN, AP1, and AP2 enhancement factors. For all calculations we took a high frequency dielectric constant $\varepsilon_\infty = 4$.

	τ (ps) BN	τ (ps) AP1	τ (ps) AP2
LDA	158.5	143.2	146.2
GGA	–	190.0	192.3
Exp.[a]	158		

[a] Reference [16].

Table 5
Positron annihilation lifetime τ in ps using the LDA approximations, the BN enhancement factor, and a high frequency dielectric constant $\varepsilon_\infty = 4$ for all the studied Al-doped ZnO systems, using the unrelaxed and relaxed structures.

Al-doped ZnO	τ (ps) Unrelaxed structures	τ (ps) Relaxed structures
ZOA(1/32)	158.8	158.6
ZOA(1/16)	158.9	159.0
ZOA(1/8a)	159.3	159.8
ZOA(1/8b)	159.3	159.5
ZOA(3/16)	159.6	160.4
ZOA(1/4a)	159.9	160.5
ZOA(1/4b)	159.9	161.7

Table 6
Positron annihilation lifetime τ in ps using the LDA approximations, the BN enhancement factor, and a high frequency dielectric constant $\varepsilon_\infty = 4$ for all the studied ZnO systems with Zn vacancies, using the unrelaxed and relaxed structures.

Zn vacancies	τ (ps) Unrelaxed structures	τ (ps) Relaxed structures
V_{Zn}(1/16)	208.9	218.9
V_{Zn}(1/8)	212.5	226.8
V_{Zn}(1/4)	235.0	248.2

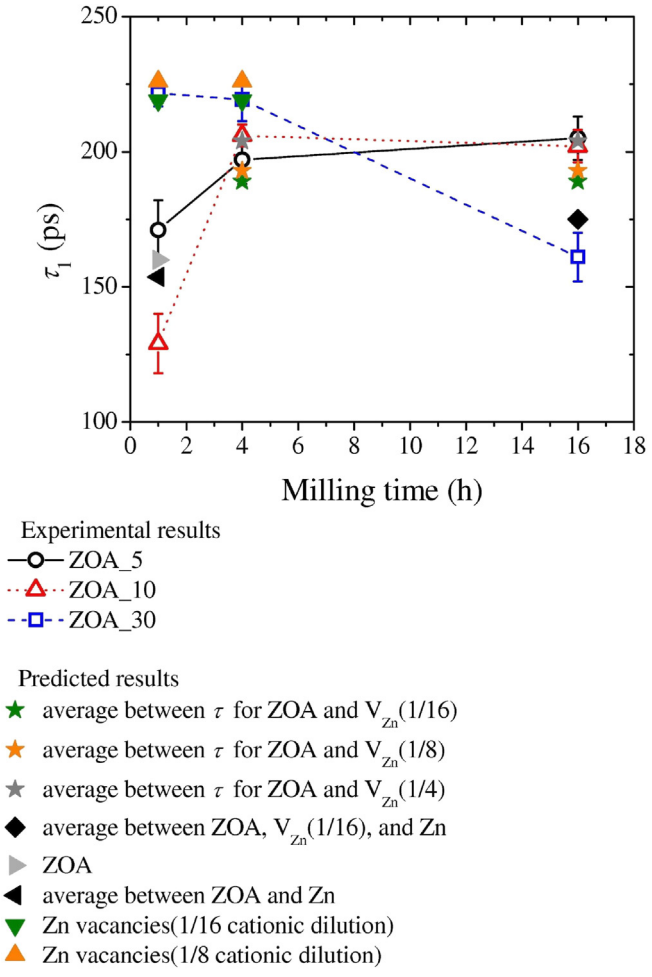

Fig. 6. Comparison between experimental results (open symbols) for τ_1 and different averages (with the same weight) of predicted positron lifetimes (closed symbols).

excellent. After 1 h of milling the lower values of τ_1 for both samples can be correlated with the absence of Zn vacancies. Particularly, τ_1 for ZOA_10 is lower than τ_1 for ZOA_5, and could be associated with the averages of the τ predicted for Al incorporated in the ZnO structure and hcp-Zn (black triangles). This presence of hcp-Zn in the ZOA_10 sample is in agreement with the observation of the XRD peak corresponding to metallic Zn that appears for this sample after 1 h of milling and that disappears after 4 and 16 h of milling (see Fig. 1). For ZOA_5, after 1 h of milling,τ_1 could be associated mainly with Al incorporated into the ZnO structure (grey triangles), also in agreement with the absence of evidence of Zn segregation in the XRD pattern for the lowest Al concentration.

On the other hand, the experimental results for ZOA_30 show a behavior which could be explain with a predominant lack of Al incorporation into the ZnO structure at substitutional cationic sites, at least at the first stages of milling. After 1 and 4 h of milling, the high τ_1 value could be related with a large formation of Zn monovacancies in undoped ZnO (the presence of a very low fraction of Al at substitutional Zn sites and also metallic Zn cannot be discarded, especially because XRD results show the developing of increasing quantities of metallic Zn in this sample). In effect, this high values for τ_1 are in perfect agreement with the prediction of Zn vacancies (orange and green triangles), but an additional combination between ZOA+metallic Zn (black triangles) and a higher concentration of Zn vacancies (V_{Zn}(1/4), see prediction in Table 6) also fits these experimental τ_1 values (not shown in Fig. 6 for clarity). Finally, after 16 h of milling the strong decrease of τ_1 could be associated with a strong segregation of hcp-Zn (in agreement with the increasing intensity of hcp-Zn peaks in the corresponding XRD patterns) together with correlated Zn vacancies, and also the additional incorporation of Al at substitutional Zn sites of the ZnO structure. In effect, it is not possible to decrease the high value of τ_1 by only increasing Zn segregation without Al incorporation, since in that way the Zn vacancies will rise at the same rate than the Zn segregation, maintaining τ_1 at a higher value than that finally observed, closer to that observed at the initial stages of milling.

It is worthwhile to note that the origin of both lifetime components (τ_1 and τ_2) in semiconductors and particularly for ZnO, takes place from the structural and morphological features of a particular sample. This is the main reason for the wide spread in bulk and trap centers positron lifetime values reported by different authors [12,15,18,34]. In our case, the obtained experimental results are consistent with reported values in the literature [12,15,20]. Moreover, our theoretically-predicted positron lifetimes values describe the general trend observed in the whole studied samples, both by XRD and PALS. Since the second component τ_2 received so many defect contributions (divacancies, vacancies agglomeration, grain boundaries, etc.) a similar theoretical analysis of τ_2 is no meaningful and goes beyond the goals of the present study.

5. Conclusions

High-energy ball milling from Al and ZnO mixtures leads to different final products according to the initial relative fractions. Al-doped ZnO nanopowders were successfully obtained up to 10 at. % of Al while for higher doping agent content a clear reduction of Zn (i.e. segregation of hcp metallic Zn) is observed.

From the *ab initio* electronic structure study for Al-doped ZnO and Zn vacancies in ZnO we could see the appearance of an extended single donor level located at the bottom of the conduction band and a double localized acceptor level located in the top of the valence band, respectively. Meanwhile, the structural full relaxation process showed that the Zn environment is higher deformed by a Zn vacancy (anisotropic increase of the distances from the Zn vacant site to its ONN atoms) than for a substitutional Al atom at the cationic site (contractions in the Al-ONN bond-lengths). The positron lifetime is strongly affected by the electronic and the structural distortions introduced by Zn vacancies while it remains practically unperturbed by those introduced by substitutional Al atoms. These two features allowed suggesting the different positron traps contribution to the observed positron lifetime evolution with milling time.

It has to be emphasized that the PALS measurements combined with state-of-the-art theoretical positron lifetime predictions can give a deeper insight into the different defect complexes and their influence in the structural and electrical properties of doped semiconductors.

Acknowledgment

This work was partially supported by Consejo Nacional de Investigaciones Científicas y Técnicas (CONICET) under Grants No. PIP0002, PIP 112-201501-00803CO, and PIP112-201101-00313, Argentina. This research made use of the computational facilities of the Physics of Impurities in Condensed Matter (PhI) group and the HPPC Bose Cluster at IFLP and Departamento de Física (UNLP). LCD, GND, and MR are members of CONICET, Argentina.

References

[1] S.J. Pearton, D.P. Norton, K. Ip, Y.W. Heo, T. Steiner, Prog. Mater. Sci. 50 (2005) 293–340.
[2] Ü. Özgür, Y.I. Alivov, C. Liu, A. Teke, M.A. Reshchikov, S. Doğan, V. Avrutin, S.-J. Cho, H. Morkoç, J. Appl. Phys. 98 (2005), 041301.
[3] A. Singh, D. Kumar, P.K. Khanna, M. Kumar, Mater. Lett. 183 (2016) 365–368.
[4] S.M. Nicaise, J.J. Cheng, A. Kiani, S. Gradečak, K.K. Berggren, Nanotechnology 26 (2015), 075303.
[5] M.D. Reyes Tolosa, L.C. Damonte, H. Brine, H.J. Bolink, M.A. Hernández-Fenollosa, Nanoscale Res.Lett. 8 (2013) 135.
[6] K.D. Kim, D.W. Choi, Y.-H. Choa, H.T. Kim, J. Mater. Process. Technol. 202 (2008) 569–573.
[7] C. Suryanarayana, N. Al-Aqeeli, Prog. Mater. Sci. 58 (2013) 383–502.
[8] L.C. Damonte, L.A. Mendoza Zélis, B. Marí Soucase, M.A. Hernández-Fenollosa, Powder Technol. 148 (2004) 15–19.
[9] L.C. Damonte, V. Donderis, M.A. Hernández-Fenollosa, J. Alloy. Comp. 483 (2009) 442–444.
[10] S. Dutta, S. Chattopadhyay, A. Sarkar, M. Chakrabarti, D. Sanyal, D. Jana, Prog. Mater. Sci. 54 (2009) 89–136.
[11] R. Krause-Rehberg, H.S. Leipner, T. Abgarjan, A. Polity, Appl. Phys. A 66 (1998) 599–614.
[12] L.C. Damonte, V. Donderis, S. Ferrari, M. Meyer, J. Orozco, M.A. Hernández-Fenollosa, Int. J. Hydrogen Energy 35 (2010) 5834–5837.
[13] J. Rodríguez-Carvajal, FULLPROF: a program for Rietveld refinement and pattern matching analysis, in: Satellite Meeting on Powder Diffraction of the XV IUCr Congress, 1990, p. 127. Toulouse, France.
[14] P. Thompson, D.E. Cox, J.B. Hastings, J. Appl. Cryst. 20 (1987) 79–83.
[15] P. Kirkegard, M. Eldrup, Comput. Phys. Commun. 7 (1974) 401.
[16] S. Dutta, S. Chattopadhyay, D. Jana, A. Banerjee, S. Manik, S.K. Pradhan, M. Sutradhar, A. Sarkar, J. Appl. Phys. 100 (2006), 114328.
[17] L.H. Su, C. Lu, L.Z. He, L.C. Zhang, P. Guagliardo, A.K. Tieu, S.N. Samarin, J.F. Williams, H.J. Li, Acta Mater. 60 (2012) 4218–4228.
[18] S.K. Sharma, P.K. Pujari, K. Sudarshan, D. Dutta, M. Mahapatra, S.V. Godbole, O.D. Jayakumar, A.K. Tyagi, Solid State Commun. 149 (2009) 550–554.
[19] R. Krause-Rehberg, H.S. Leipner, Positron Annihilation in Semiconductors: Defect Studies, Springer, Heidelberg, Germany, 1999.
[20] F. Tuomisto, K. Saarinen, D.C. Look, G.C. Farlow, Phys. Rev. B 72 (2005), 085206.
[21] E.H. Kisi, M.M. Elcombe, Acta Cryst. C 45 (1989) 1867–1870.
[22] G.K.H. Madsen, P. Blaha, K. Schwarz, E. Sjöstedt, L. Nordström, Phys. Rev. B 64 (2001), 195134.
[23] P. Blaha, K. Schwarz, G. Madsen, D. Kvasnicka, J. Luitz, WIEN2k, an Augmented Plane Wave Plus Local Orbitals Program for Calculating Crystal Properties, Technical Universität, Wien, Austria, 2012.
[24] J.P. Perdew, Y. Wang, Phys. Rev. B 45 (1992) 13244–13249.
[25] J.P. Perdew, K. Burke, M. Ernzerhof, Phys. Rev. Lett. 77 (1996) 3865–3868.
[26] B. Kohler, S. Wilker, M. Sheffler, R. Couba, C. Ambrosch-Draxl, Comput. Phys. Commun. 94 (1996) 31–48.
[27] T. Torsti, M. Heiskanen, M.J. Puska, R.M. Nieminen, Int. J. Quant. Chem. 91 (2003) 171–176.
[28] M.J. Puska, R.M. Nieminen, J. Phys. F Met. Phys. 13 (1983) 333–346.
[29] E. Boronsky, R.M. Nieminen, Phys. Rev. B 34 (1986) 3820–3831.
[30] J. Arponen, E. Pajanne, Ann. Phys. 121 (1979) 343–389.
[31] B. Barbiellini, M.J. Puska, T. Torsti, R.M. Nieminen, Phys. Rev. B 51 (1995) 7341–7344.
[32] G.N. Darriba, E.L. Muñoz, L.A. Errico, M. Rentería, J. Phys. Chem. C 118 (2014) 19929–19939.
[33] J. Kuriplach, B. Barbiellini, J. Phys. Conf. 505 (2014), 012040.
[34] S.K. Neogi, R. Karmakar, A.K. Misra, A. Banerjee, D. Das, S. Bandyopadhyay, J. Magn. Magn Mater. 346 (2013) 130–137.